Comparison of the Structure of the ITCZ in the West Pacific during the Boreal Summers of 1989–93 Using AMIP Simulations and ECMWF Reanalysis

S. C. CHAN AND J. L. EVANS

The Pennsylvania State University, University Park, Pennsylvania

(Manuscript received 11 December 2001, in final form 23 May 2002)

ABSTRACT

The dynamic structure and interannual variability of the ITCZ in the western North Pacific and east Asia during the boreal summers of 1989–93 are investigated. European Centre for Medium-Range Weather Forecasts (ECMWF) reanalyses are used to characterize the dynamical structure of the ITCZ. The ITCZ structure in the National Center for Atmospheric Research (NCAR) Community Climate Model 3 (CCM3.6) and the National Aeronautics and Space Administration (NASA) Goddard Institute of Space Studies (GISS) SI2000 GCM is also explored.

The ITCZ axis can be partitioned into three sections in the western North Pacific and east Asia: the continental monsoon trough (CMT) in India, the Bay of Bengal, and Indo-China; the oceanic monsoon trough (OMT) in the Pacific warm pool; and the trade wind trough (TWT) in the central Pacific. The confluence point (CP) is defined as an area where the broad cyclonic flow in OMT changes to the easterly trades of the TWT. East of the CP, both GCMs simulate a weaker easterly trade wind regime with a broader ITCZ due to the dislocation of the Pacific high. To the west of the CP, both GCMs simulate a weaker cross-equatorial flow and OMT. Both models show skill in simulating the interannual variability of the location of the CP; however, for the peak ENSO warm phase years (1992–93), the spread among ensemble members of the CP longitude is comparable to the shift of ensemble mean CP location relative to 1989. That is, the internal variability of each GCM is on the same order as the simulated interannual variability in this region.

1. Introduction

One-third of the earth's surface is directly affected by the seasonal cycle of the Asian summer monsoon and Pacific ITCZ. The locations of the ITCZ and monsoon trough play a critical role in determining the flow and the precipitation patterns, tropical cyclone evolution, and the hydrologic cycle of this region. A common method for evaluating the skill of general circulation models in the tropical west Pacific (WPAC) and the east Asian monsoon region is by validating a time-averaged climatology (Gadgil and Sajani 1998; Lau and Li 1984; Meehl and Arblaster 1998). One issue that could arise from such a time average is the smearing out of the seasonal cycle and intraseasonal oscillations. In the WPAC, the seasonal cycle of the Asian and the tropical west Pacific monsoon strongly influences the dynamics and precipitation patterns of the region (Lau and Li 1984; Wu and Wang 2001). Although intraseasonal oscillations like the Madden–Julian oscillation (MJO; Madden and Julian 1972) and equatorial Rossby and Kelvin waves (Matsuno 1966) have shorter periods than the seasonal cycle, they also play a role in the dynamics and rainfall in the tropical and subtropical WPAC (Wheeler et al. 2000).

Our goal has been to develop a time-averaging technique that preserves the effects of these oscillations and the seasonal cycle as well as possible. One possible technique for reducing the effect of the smearing is through ITCZ and (ocean) monsoon trough (OMT) compositing. By centering all variables of interest on to the ITCZ and OMT axis, one can improve the structural detail of these two features. This technique is employed here to analyze GCM simulations and to compare them with observations.

The objective of this study is to compare a composite wind field structure of the ITCZ and monsoon trough of two specific Atmospheric Model Intercomparison Project (AMIP) GCM ensemble simulations with observations. Eighteen GCMs from different international institutes participate in the AMIP project. The AMIP project (Gates et al. 1999) is a concentrated international effort to facilitate GCM development and is supported by the Working Group on Numerical Experimentation of the World Climate Research Programme.

The two GCMs used in this study are the National Aeronautics and Space Administration (NASA) Goddard Institute for Space Studies (GISS) SI2000 GCM

Corresponding author address: Dr. Jenni Evans, Department of Meteorology, The Pennsylvania State University, 503 Walker Bldg., University Park, PA 16802-5013.
E-mail: evans@essc.psu.edu

(Hansen et al. 1997) and the National Center for Atmospheric Research (NCAR) Community Climate Model 3.6 (CCM3) GCM (Kiehl et al. 1996, 1998). These two GCMs are compared with diagnostics derived from the European Centre for Medium-Range Weather Forecasts (ECMWF) reanalysis (Gibson et al. 1997). The region of interest lies between 20°S–35°N and 110°–195°E; this area covers the tropical central Pacific (CPAC) and the WPAC, as well as most of Asia. The WPAC and the CPAC are areas of active and frequent convection, and together combine to cover about one-fifth of the globe. Accurate simulation of the climate of these areas has important implications for the model-simulated global heat budget and hydrological cycle. The WPAC and the CPAC also play an active role in tropical interannual variability due to ENSO-related SST anomalies; the ability of the models to handle ENSO has important implications for the interannual variability of the model-simulated climate.

Deficiencies in the precipitation patterns of general circulation models in the tropical west Pacific and the Asian monsoon region are well documented in the literature (Gadgil and Sajani 1998; Lau et al. 1996). These deficiencies include the lack of precipitation migration toward the Asian continent during the Northern Hemisphere summer (i.e., the main rainband remains near the equator, etc; Gadgil and Sajani 1998; Lau et al. 1996), and model deficiencies in simulating the interannual variability in the WPAC and the Asian monsoon region (Meehl and Arblaster 1998). The causes of these deficiencies can be related to the cumulus parameterization (Slingo et al. 1994), the hydrological parameterization (Laval et al. 1996), topographic representation (Fennessy et al. 1994), horizontal resolution (Sperber et al. 1994), or feedbacks from the wind fields (Meehl and Arblaster 1998).

Ramage (1971) and Chang and Chen (1995) demonstrated the importance of monsoon southwesterly flow in the Asian monsoon region on monsoon precipitation onset; the first arrival of a low-level southwesterly jet is followed by the onset of monsoon rains during boreal spring–summer. Meehl and Arblaster (1998) discussed the impact of low-level convergence in the difference between the precipitation fields near the Philippines from the Climate System Model (CSM; a version of CCM3 coupled with an ocean model) and CCM3 forced by the observed AMIP SST. The CSM develops stronger low-level convergence and significantly more rainfall than the AMIP–SST-forced CCM3, highlighting the importance of accurate simulation of the dynamics in the WPAC and east Asia to the GCM simulated rainfall.

Mapes and Houze (1995) demonstrated the importance of feedback from deep convection to the large-scale flow field in the Tropics: gravity wave modes generated by deep convection in the Tropics can significantly weaken the easterly trade wind flow; therefore, excess tropical rainfall can potentially weaken the easterly trades. Thus, wind field differences between the GCMs and observations could be caused by (but not limited to) the feedback from the cumulus parameterization of the model or model-simulated wind fields.

Improvements in GCM simulations are critical for climate prediction, and to understand the possible impact of human-induced climate change and natural climate variability. Identification of the strengths and weaknesses in the wind field structure of the two GCMs provides indications of relative model skill and areas for future GCM improvement. The monsoon–ITCZ composite approach developed by Briegel and Frank (1997) and that is demonstrated here provides an alternative approach to standard time averaging for validating regions with high inter- and intraseasonal variability.

2. Motivation

Identification of GCM biases is a method of documenting the development of these sophisticated models. The compositing technique employed in this study provides an alternative way to understand GCM skill. Instead of a time-mean field that smears out the variability in the Tropics, the technique evaluates GCM ability to simulate the day-to-day ITCZ structure in the tropical west Pacific. Such technique can also be applied to other GCMs and observation datasets.

GCMs are designed to be a tool in climate prediction. Therefore, understanding GCMs biases (and its implications) is a useful tool for climate forecasters. ENSO events are associated with low-level zonal wind anomalies in the central tropical Pacific; zonal wind biases in the tropical Pacific may imply the simulated climatologies are favoring a specific ENSO phase. The background low-level vorticity in the monsoon trough makes that area favorable to tropical cyclogensis (Gray 1968). Anomalous wind fields and vorticity in the monsoon trough in GCMs may make GCM climatologies look more favorable/unfavorable to tropical cyclones. In order to forecast extreme climate events skillfully with GCMs, GCMs must show they have skill to produce reasonable environmental wind patterns and rainfall estimates.

Convection and wind fields in the Tropics play an important role in global atmosphere and ocean energy budgets. This study involves a significant fraction of the tropical Pacific from 110°E to 160°W (about one-fifth of the surface of the globe). Accurate GCM simulations of the rainfall and wind field for such large and critical area have important implications to the global energy budgets.

3. Observed WPAC ITCZ structure

Observations show the general flow structure in the WPAC can be divided into two main regimes (Briegel and Frank 1997; Holland 1995): the easterly trade wind trough (TWT) and the oceanic monsoon trough (OMT). A schematic of the flow in WPAC is shown in Fig. 1.

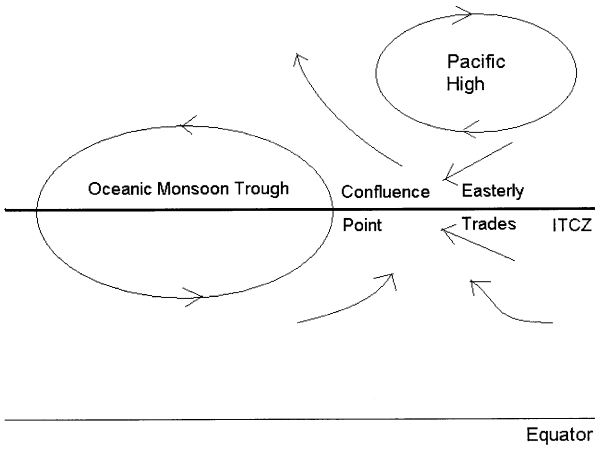

FIG. 1. Schematic model of the summer Tropics. Typical lower-troposphere flow near the CP and the OMT. The CP is defined as the point where the flow turns from an easterly trade (TWT) to a broad cyclonic flow (OMT) in the western Pacific Ocean. East of the CP, the easterly trade wind marks the TWT; precipitation in TWT is confined to a narrow band between 5° and 10°N due to the large-scale sinking motion in the Pacific high and equatorial ocean upwelling (Philander et al. 1996). West of the CP, a broad cyclonic flow marks the OMT; in the OMT, warm ocean and background supports frequent tropical cyclone activity (Gray 1968).

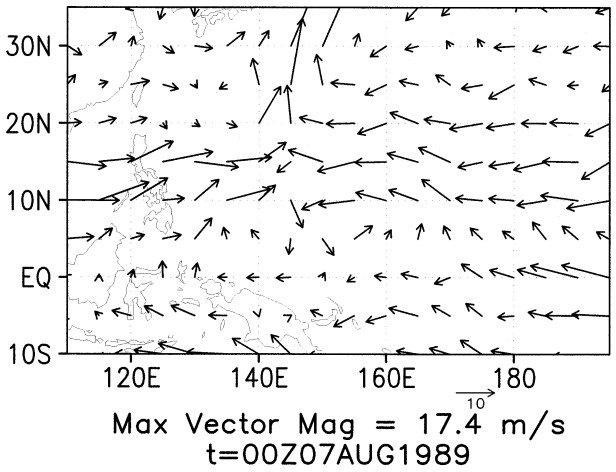

FIG. 2. ECMWF reanalysis 850-hPa wind vectors for 0000 UTC 7 Aug 1989 in the tropical west Pacific region. The domain plotted represents the region of interest for this study: 10°S–40°N, 110°E–160°W.

The TWT and OMT are driven by the meridional temperature gradients between the equator and the subtropics and modulated by convection and land–sea contrasts. The TWT is associated with shear vorticity and large-scale low-level convergence. Weather in the TWT is associated with narrow band of scattered deep convection (Waliser and Gautier 1993). North of the TWT is a broad subtropical high pressure system (the Pacific high). The Pacific high is characterized by large-scale sinking motion, which inhibits deep convection.

The confluence point (CP) is defined as an area (identified via a central latitude–longitude point) where flow changes from easterly trade winds into a cyclonic flow with near-equatorial monsoon westerlies in the OMT (Fig. 1). The CP has been hypothesized as a region of Rossby–gravity wave energy trapping in the upper troposphere (Chang and Webster 1990). Observations show the CP is a favorable area for tropical cyclogenesis (Briegel and Frank 1997; Ritchie and Holland 1999).

The OMT is defined as an area of broad cyclonic flow west of the CP in the west Pacific warm pool. Near-equatorial monsoon westerlies/southwesterlies lie south of the OMT axis, and easterlies north of the OMT axis. The cyclonic flow is enhanced by diabatic heating associated with latent heat release from the deep convection in the region (Webster 1981; Holland 1995). When the OMT is far from the equator during boreal summer and fall, it is a favorable area of tropical cyclogensis; this is because of the high low-level background vorticity, the warm SST, and the prevalence of deep convection in the OMT (Gray 1968). Briegel and Frank (1997) and Ritchie and Holland (1999) found that 70% of the tropical cyclone genesis cases in the WPAC occur in the OMT near the CP.

To the west of the OMT, the continental monsoon trough is a low pressure trough dominated by intense differential radiative heating in continental Asia, due in part to the elevated heat source of the Himalayan Plateau at about 500 hPa. It is associated with a low-level (850 hPa) monsoon cross-equatorial southwesterly flow driven by the pressure gradient with the Southern Hemisphere's low-level cold high pressure system formed due to radiative cooling during austral winter.

In order to illustrate the schematic, it is compared with actual observations. The ECMWF reanalysis 850-hPa wind vectors for 0000 UTC 7 August 1989 over the region of interest are shown in Fig. 2. Easterly trade winds dominate the area east of 170°E. The monsoon trough extends from the Asian continent to about 170°E. The CP is located at about 5°N, 170°E. The monsoon trough appears to be broken into two segments; the first segment extends from the Asian continent to about 20°N, 145°E, and another segment is from 5°N, 145°E to the CP. The latter segment is associated with Tropical Depression Owen, whose center is located around 7.5°N, 150.8°E (Plante and Guard 1989).

4. Models and observational data description

Out of the 18 GCMs that are involved in the AMIP project, only two are evaluated here due to time and resource constrains. The two GCMs are the NCAR CCM3.6 (Kiehl et al. 1996, 1998) and the NASA-GISS SI2000 (Hansen et al. 1997). The CCM3 runs in this study were also used in the regional climate modeling study of Dutton and Barron (2000). The NASA-GISS SI2000 GCMs were provided by the courtesy of Dr. Hansen and his research group at NASA-GISS.

Both sets of model ensembles use ''standard'' model

physics (i.e., no change of any physical parameterization to test model sensitivity). They are all forced by observed AMIP SST (Reynolds and Smith 1994; Smith et al. 1996). Six CCM3 and five SI2000 simulations that differ only in details in their initial conditions are studied here: each CCM3 ensemble member starts on a different day of the same month of the ''spinup'' run; all SI2000 ensemble members start at the same day, but with slightly different initial conditions created by adding small random perturbations to the spinup run (K. K.-W. Lo 2000, personal communication).

The CCM3 runs have a T31 spectral truncation, which gives a coarser horizontal resolution than the standard CCM3 T42 spectral truncation. This study is not intended to understand the sensitivity of CCM3 to different spectral truncations or horizontal resolutions. Past studies in earlier versions of the Climate Community Model have looked into model sensitivity to horizontal resolution (Boville 1991; Kiehl and Williamson 1991). Kiehl and Williamson (1991) have found that vertical motions in the Tropics become more vigorous in higher resolutions; higher-resolution runs have a deeper moist ascent in the Tropics, and a better defined subtropical sinking branch.

CCM3 uses Zhang and McFarlane (1995) ensemble plume deep convection parameterization. Deep convection is possible if the lower troposphere is conditionally unstable, and convection acts to remove convective available potential energy (CAPE) at an exponential rate. A separate scheme (Kiehl et al. 1996) is used to handle shallow and midtroposphere convection. Boundary layer and surface physics is based on ''nonlocal'' turbulent transport (Holtslag and Boville 1993) in which turbulent mixing is proportional to vertical gradients and eddy diffusivity (Deardorff 1972). Eddy diffusivity is a function of the boundary layer height, H; H depends on the bulk Richardson number, adjusted to account for shear production of turbulence due to surface friction (Vogelezang and Holtslag 1996). The solar constant is fixed at 1367 W m^{-2}, and the model has a diurnal cycle. There are six CCM3 ensemble member runs with T31 spectral truncation (about 3.75° latitude $\times$ 3.75° longitude) and 18 hybrid vertical levels up to 4.8 hPa.

SI2000 uses the Del Genio and Yao (1993) convection scheme. Convection is allowed if air parcels become buoyant when they are lifted to the vertical layer above. This scheme assumes there is just enough mass flux to restore buoyant instability in one hour. This scheme includes precipitation evaporation, convective downdraft, and anvil and stratiform precipitation. Unlike CCM3, the cumulus parameterization in SI2000 does not treat deep and shallow convection separately. SI2000 uses Hartke and Rind (1997) boundary layer physics, employing similarity theory to calculate transport and drag coefficients. The model has a diurnal cycle with variable solar irradiance that includes effects from sunspot cycles (Lean 2000). Model spinup for the five ensemble members is forced by climatological SST from the Hadley Centre (Rayner 2000). SI2000 is a gridpoint model with a 4° latitude $\times$ 5° longitude horizontal resolution, and 12 vertical sigma levels. The details of the model numerical techniques are described in Abramopoulos (1991).

The ECMWF reanalysis (Gibson et al. 1997) has a spectral truncation of T42, which corresponds to a horizontal resolution of about 2.5° latitude $\times$ 2.5° longitude. The analyses have 31 hybrid vertical levels, but only the 850-hPa level is used in this study. Data are available every 6 h at 0000, 0600, 1200, and 1800 UTC. The dataset is a combination of global ground and satellite observations and ECMWF operational model simulations. Earlier studies have suggested ECMWF reanalysis is better than the NCEP reanalysis in the Tropics (Trenberth and Guillemot 1998; Engelen et al. 1998; Newman et al. 2000). Trenberth et al. (2001) finds that ECMWF reanalysis shows temperature discontinuity around October–November 1986 and March–April 1989, and the discontinuity might adversely affect the usefulness of the ECMWF reanalysis to long-term climate studies. The results here are based on June–September of 1989 and 1992, and therefore the temperature discontinuity will have no effect on the results presented here.

5. Definitions and methodology

The methodology of this compositing study can be divided into two main components: the determination of the location of the ITCZ axis and the CP location, and construction of the composite. The methodology is outlined in this section, but precise definitions of certain terms are given first.

a. Definition of the ITCZ and WPAC monsoon onset

There is a lack of a standard definition of the ITCZ (Sadler 1975). The ITCZ has been defined as near-zonal line of tropical convection, and/or pressure trough, and/or a low-level wind confluence line (Gadgil and Guruprasad 1990; Waliser and Gautier 1993; Sadler 1975). In this study, the ITCZ axis is defined to be a (near zonal) line of 850-hPa relative vorticity maxima in between the equator and 30°N. The TWT and OMT are distinguished at the CP; the ITCZ axis to the east of the CP is the TWT, and the ITCZ axis to the west of the CP is the OMT.

ITCZ compositing only includes the time between WPAC monsoon onset and retreat. In this study, the WPAC monsoon onset (retreat) is defined to be the development (withdrawal) of a sustained (at least 4 days) 850-hPa westerly wind component east of 125°E between 10° and 15°N. This dynamically based definition is similar to the onset definition used in Lau and Yang (1996). Observations show the arrival of monsoon rains occurs immediately after the arrival of monsoon southwesterlies (Lau and Li 1984; Tao and Chen 1987). Both

the onset and the retreat dates are determined by finding the onset and retreat of sustained monsoon southwesterlies visually using zonal wind Hovmoeller diagrams. The WPAC monsoon onset time and retreat time for the ECMWF reanalysis and the individual ensemble members in the two GCMs are shown in Fig. 3. For the 5 yr of interest (1989–93), the onset time for the ECMWF reanalysis is mid- to late June, and the retreat time is mid-September and beyond. According to Wu and Wang (2001), the typical onset time of WPAC monsoon in the Philippine Sea is between 15 and 19 June; the observed onset dates plotted in Fig. 3 agree well with Wu and Wang's results. For CCM3, the typical onset time is usually mid- to late June, the 5-yr ensemble mean onset time is 16 June, similar to the 5-yr mean ECMWF reanalysis onset time (18 June). For the 1992 ENSO year, the onset time is as late as early July for individual ensemble members. The ensemble member spread of monsoon onset time is on the order of 1 month. SI2000 has onset times earlier than both CCM3 and the ECMWF reanalysis. All SI2000 ensemble members have onset times for 1989 before 1 June, prior to the time of interest in this study. The SI2000 ensemble mean 4-yr-average monsoon onset time between 1990 and 1993 is 10 June, which is about 1 week earlier than CCM3 and the ECMWF reanalysis onset times. Inclusion of 1989 in the time average makes the difference larger; the ensemble mean 5-yr-average SI2000 monsoon onset time between 1989 and 1993 is 5 June.

b. ITCZ axis and CP location determination technique

A brief outline of the methodology will be given here. Further details on how the ITCZ axes are determined are given in the appendix and in Chan (2001).

The ITCZ axis (including OMT, CP, and TWT) is defined to be an elongated line of 850-hPa relative vorticity maximum. Beginning from the east most longitude of interest (160°W), a rule-based routine determines a near-zonal line of vorticity maximums (the ITCZ) between the equator and 30°N for each time period of interest. Two major methods are used to determine the ITCZ—the ''well-defined'' trough scheme, and the ''poorly defined'' trough scheme (Chan 2001).

After the ITCZ axis is completely defined for one time period, the CP is determined by finding a shift from easterly trades to westerlies south of the ITCZ axis. The shift from easterlies to westerlies marks the transition from a trade wind regime to a cyclonic flow regime that is associated with the monsoon trough.

c. ITCZ axis compositing technique

Refer to the appendix or Chan (2001) for details on how the composites are constructed. An outline of the composite technique is given here.

The mean location of all the CP of each time period

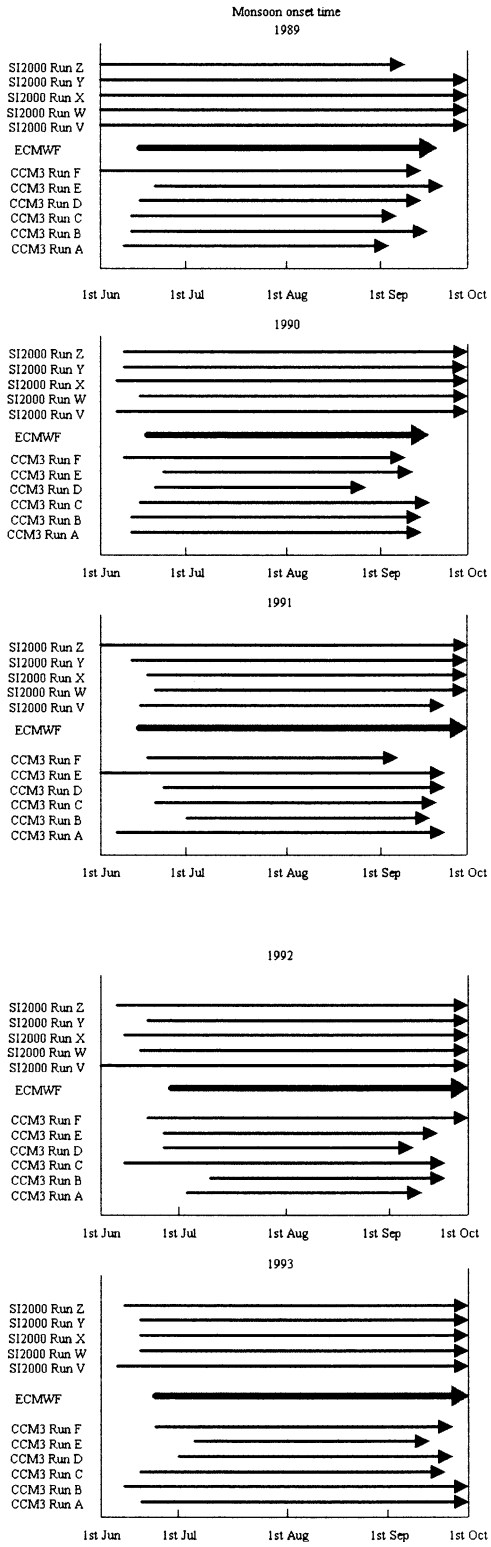

FIG. 3. 1989–93 west Pacific monsoon onset and retreat times for the ECMWF reanalysis (heavy arrow), the SI2000 ensembles, and the CCM3 ensembles.

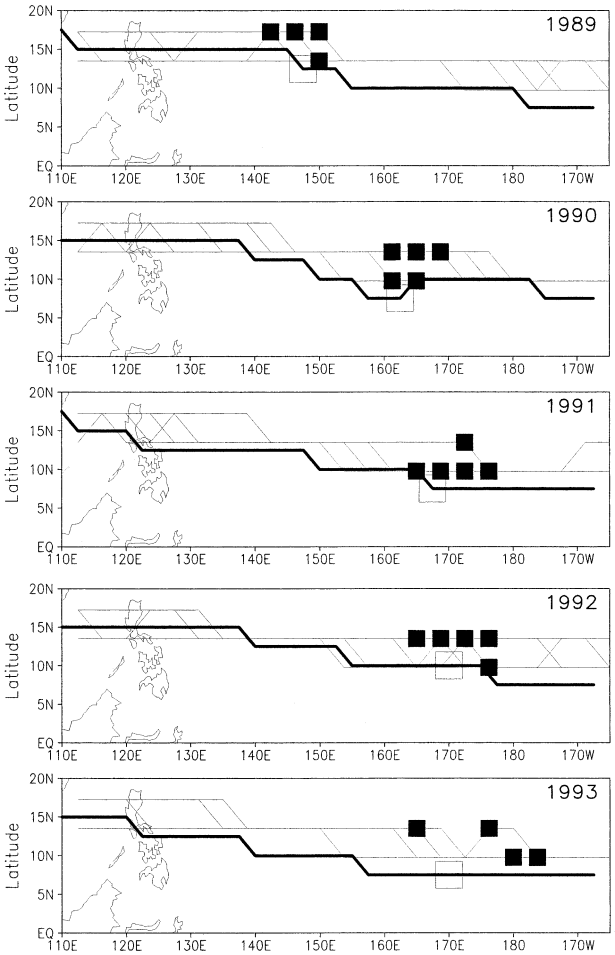

FIG. 4. Time-averaged CP location and composite ITCZ axis for observations and each CCM3 ensemble member. The single thick line and hollow square are the ITCZ axis and CP location, respectively, from the ECMWF reanalysis, and the thin lines and solid squares are the ITCZ axis and CP location for each of the CCM3 ensemble members.

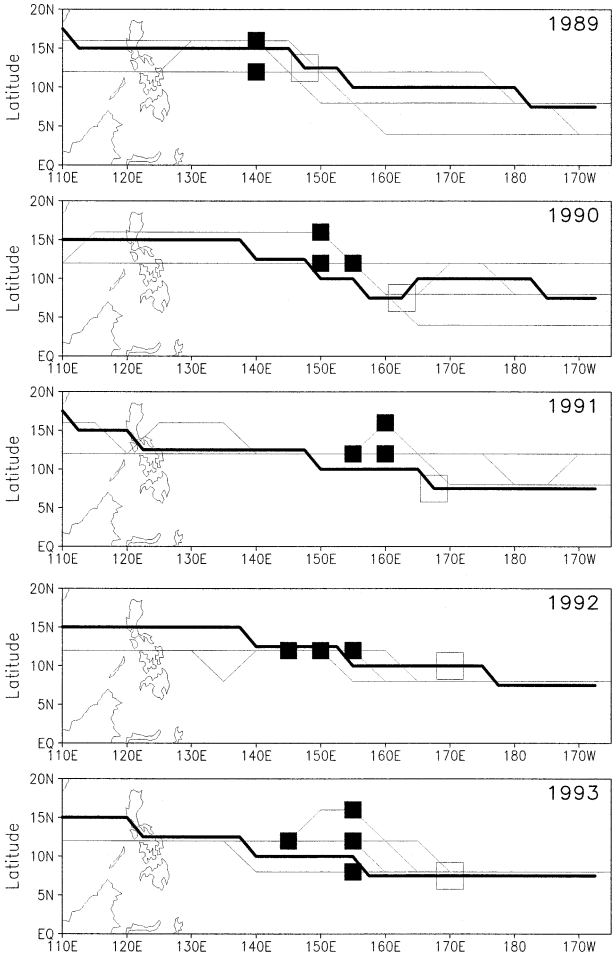

FIG. 5. Time-averaged CP location and composite ITCZ axis for observations and each SI2000 ensemble member. The thick line and hollow square are the analyses' ITCZ axis and CP location, respectively, and the thin line and solid square are the SI2000 ensemble members ITCZ axis and CP location, respectively.

of interest are calculated. The 850-hPa winds at each time period's CP are then centered onto the mean CP location. Once each ITCZ axis is centered onto the mean CP, a composite mean ITCZ axis can be calculated. Since the centered ITCZ axis for each different time period differs with the composite mean ITCZ axis, the wind maps and ITCZ axis of each time period is moved meridionally onto the composite mean ITCZ axis. With all wind maps now centered onto the composite mean ITCZ, a composite mean wind map can now be calculated by simply by averaging across all of these centered wind maps.

6. The location of the composite ITCZ axis and the confluence point for 1989–93

Before exploring the difference in ITCZ structure between GCMs and observations, the differences between the CP and ITCZ axis locations between the ECMWF reanalysis and the GCMs and their interannual variability are first discussed. The composite ITCZ axis and time-mean CP location for each CCM3 (Fig. 4) and SI2000 (Fig. 5) ensemble member and ECMWF reanalysis for 1989–93 (superimposed on all plots) are shown. The latitude and the longitude (rounded to the nearest grid point) of the CP for those years are shown in Tables 1 and 2, respectively. The analyses show that the ECMWF reanalysis CP moves eastward toward CPAC from 1989 to 1993 due to westerly zonal wind anomalies in the equatorial Pacific related to positive SST anomalies in EPAC/CPAC during the prolonged El Niño event in the early 1990s.

a. CP and ITCZ locations in CCM3

CCM3 showed skill in simulating the eastward movement of the CP from 1989 to 1993 (Fig. 4), and shows

TABLE 1. Latitude of CP for ECMWF reanalysis, CCM3, and SI2000 ensemble members.

	1989	1990	1991	1992	1993
ECMWF	12.5°N	7.5°N	7.5°N	10°N	7.5°N
CCM3 (a)	17.25°N	13.5°N	9.75°N	13.5°N	9.75°N
CCM3 (b)	17.25°N	9.75°N	9.75°N	13.5°N	13.5°N
CCM3 (c)	13.5°N	13.5°N	9.75°N	13.5°N	13.5°N
CCM3 (d)	13.5°N	13.5°N	9.75°N	9.75°N	9.75°N
CCM3 (e)	17.25°N	13.5°N	9.75°N	13.5°N	9.75°N
CCM3 (f)	13.5°N	9.75°N	13.5°N	13.5°N	9.75°N
SI2000 (V)	16°N	12°N	12°N	12°N	12°N
SI2000 (W)	12°N	12°N	12°N	12°N	12°N
SI2000 (X)	16°N	16°N	16°N	12°N	8°N
SI2000 (Y)	16°N	12°N	12°N	12°N	12°N
SI2000 (Z)	16°N	12°N	12°N	12°N	16°N

no systematic bias in the location of the longitude of the CP. The longitudinal spread of CP among ensemble members is higher during 1991, 1992, and 1993 (11.25° for 1991 and 1992, and 18.75° for 1993) than 1989 and 1990. This CP ensemble location spread is comparable to the eastward movement of ensemble mean CP longitude of 23° for 1992 and 30° for 1993 (cf. each case to 1989). CCM3 has a north bias of 1°–6° latitude in CP location for every year and for all ensemble members, with the spread of latitudes of CP among ensemble members for any year is no more than 4°.

CCM3 captures the observed northwest–southeast tilt of the ITCZ axis (Fig. 4). With the exception of 1990, the CCM3 ITCZ axis is more zonal than the analyses, resulting in a north bias in the ITCZ axis of 3°–6° latitude near and east of the CP in the TWT. This northward ITCZ axis bias covers nearly the whole domain for 1993, and for 1991. For other years (1989, 1990, 1992), the ITCZ north bias extends westward to about 135°–145°E; farther westward, the simulated ITCZ is more or less the same latitude as in the analyses. The ensemble member spread of ITCZ axis latitude is no more than 3°–4° (one meridional grid point) in the OMT and TWT.

b. CP and ITCZ locations in SI2000

SI2000 simulates the interannual variability of the CP from 1989 to 1993 well, but the simulated CP location consistently has a west bias of 10°–20° longitude in every year (relative to the ECMWF reanalysis; Fig. 5). The ensemble member spread of CP longitude is larger for 1992 and 1993 than the other years (similar to CCM3). The longitudinal spread of the CP for 1992 and 1993 (about 10°) is comparable to the peak interannual displacement of the ensemble mean CP location from 1989 to 1992/93 of 10°–15°. There is a north bias of CP latitude every year except 1989 and 1992. This CP north bias in SI2000 is no more than 6°, and the ensemble member spread of CP latitude is no more than 8° (i.e., two grid points).

The ITCZ axis in SI2000 also displays a northwest–southeast tilt. For 1991–93, the ITCZ axis tilt is less than both the ECMWF analyses and CCM3, resulting in a more zonal ITCZ axis. It is shown in Chan (2001) that the latitudinal bias of the ITCZ axis east of 120°E (relative to the analyses) of SI2000 is less than the latitudinal bias in ITCZ axis bias over India. For other years, there are no clear northward or southward biases in ITCZ axis location east of 120°E except 1991; in 1991, the simulated ITCZ axis is always north of the analysis ITCZ axis east of 150°E. The latitudinal spread of the ITCZ axis among SI2000 ensemble members is no more than 8° (two grid points) for all years. The ITCZ axis spread is the largest for the axis east of the CP during 1989 and 1990; the ensemble member spread of the ITCZ axis east of the CP is up to 8° latitude for those two years. For 1993, the largest ITCZ axis spread occurs west of the CP near 150°–155°E.

7. The 850-hPa ITCZ axis structure for 1989 and 1992

The years 1989 and 1992 have been chosen for in-depth analysis and intercomparison of the ITCZ structure. 1989's boreal summer is a period during which the La Niña conditions during 1988/89's boreal winter are giving way to a prolonged El Niño period that lasted from 1990 to 1994; the time-averaged Southern Oscillation index (SOI) during the boreal summer (June–September) of 1989 is 0.28 (Columbia University 2001), indicating neutral to colder-than-normal SST conditions.

TABLE 2. Longitude of CP for ECMWF reanalysis, CCM3, and SI2000 ensemble members.

	1989	1990	1991	1992	1993
ECMWF	147.5°E	162.5°E	167.5°E	170°E	170°E
CCM3 (a)	150°E	165°E	168.75°E	165°E	183.75°E
CCM3 (b)	146.25°E	165°E	165°E	168.75°E	165°E
CCM3 (c)	150°E	165°E	176.25°E	168.75°E	176.25°E
CCM3 (d)	150°E	161.25°E	172.5°E	176.25°E	183.75°E
CCM3 (e)	142.5°E	168.75°E	168.75°E	176.25°E	180°
CCM3 (f)	150°E	161.25°E	172.5°E	172.5°E	183.75°E
SI2000 (V)	140°E	150°E	155°E	155°E	145°E
SI2000 (W)	140°E	155°E	155°E	150°E	155°E
SI2000 (X)	140°E	150°E	160°E	145°E	155°E
SI2000 (Y)	140°E	150°E	160°E	155°E	155°E
SI2000 (Z)	140°E	150°E	160°E	150°E	155°E

The year 1992 is within a prolonged El Niño event; the time-averaged SOI during the boreal summer (June–September) is −0.50, consistent with the warmer-than-average SST conditions. Although neither period shows extreme SST conditions (the magnitude of SOI is bigger than 1.0), the magnitude of the SOI index during the boreal winter at the beginning of each year is large. The SOI peaks at about +2.0 on the boreal winter just before the boreal summer of 1989, and the SOI sinks to about −3.5 on the boreal winter before the boreal summer of 1992. The use of 1989 and 1992 can then give a sense of the impact of interannual variability to the ITCZ structure in the WPAC.

The discussion here focuses on the ensemble member variability of the ITCZ structure in the two different GCMs, and the ensemble mean vector wind differences between the observed ECMWF reanalysis 850-hPa wind composite and the GCM (CCM3 and SI2000) composites. As documented in section 4, there are considerable differences in the ITCZ and CP locations among the GCMs and the ECMWF reanalysis. Thus, direct subtraction of the GCM vector fields from the ECMWF reanalysis field is likely to be masked by the difference of the ITCZ locations. In order to reduce the impact of this location bias in assessing structural differences, all GCM ensemble member composites are centered onto the ECMWF reanalysis ITCZ axis and CP location before subtraction.

a. Composite ITCZ structure for JJAS 1989

The ITCZ composites for 1989 is first evaluated by comparing the composite maps of both the ECMWF reanalysis and the GCMs. The vector difference fields between the ECMWF reanalysis composites and the GCM composites are then evaluated.

Vector wind composites at 850 hPa for ECMWF reanalysis, CCM3 ensemble members, and SI2000 are shown in Figs. 6, 7, and 8, respectively. Individual ensemble members of both the GCMs and the ECMWF reanalysis show a well-defined OMT bounded by the CP on the east, in good agreement with the ITCZ schematic shown in Fig. 1. Near the CP, westerly monsoon flow turns sharply northward into a southeasterly wind. East of the CP, it is dominated by the easterly trades. North of the trades, there is a broad subtropical anticyclonic (Pacific high), but the Pacific high represented in the GCMs is always located farther northeast than observed—a result that is clear from the composite differences (Fig. 9). South of the OMT, the flow is dominated by the cross-equatorial southerly flow associated with the Asian monsoon.

Some clear differences can be seen between the ECMWF reanalysis composites and the GCM composites. Both GCMs show stronger southerly meridional flow than observed in the TWT. This stronger meridional flow is likely related to positive precipitation anomalies in subtropical CPAC (Fig. 10), and can be seen as a cyclonic anomaly over CPAC in the composite vector difference (to be discussed later). The westerly monsoon flow south of the OMT is weaker in the GCMs, which can also be seen in composite vector difference (to be discussed later).

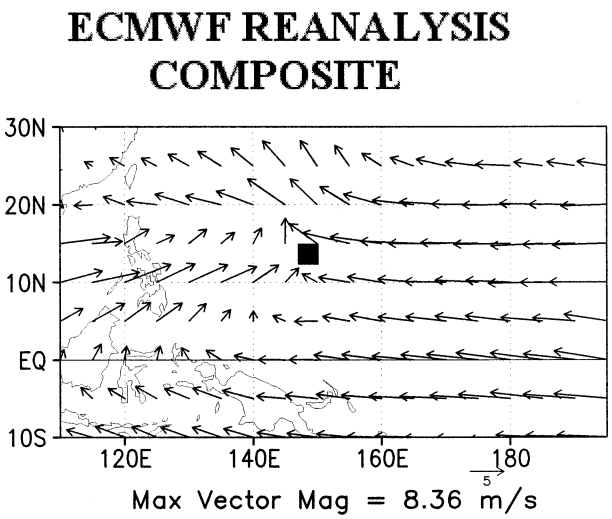

FIG. 6. ECMWF reanalysis 850-hPa wind composite for 1989. The solid square denotes the mean CP location for the season.

Noticeable ensemble member variability is seen in the OMT in the SI2000 composites. Hovmoeller diagrams of zonal wind (not shown) show tropical wave–like structures with periods and phase speed close to equatorial Rossby waves in SI2000 ensembles. The periods of these waves are on the order of 15–30 days with typical westward phase speed of 2.5–5 m s^{-1}. Since the periods of these wavelike structures are comparable to the period of compositing (4 months), the effects of these waves may be contributing to this ensemble member variability in SI2000. That is, the choice of compositing to analyze the ITCZ structure on timescales of weeks to months may capture some of the large-scale wave activity represented by the GCM, enhancing the ensemble member spread compared to traditional time averaging (see Chan 2001).

Ensemble mean vector differences between GCM ensemble members and the ECMWF reanalysis for 1989 are shown in Fig. 9. As mentioned earlier, GCM composites are first centered onto the ECMWF reanalysis composites before subtraction. The difference is computed for each GCM ensemble member. Finally, the ensemble mean difference is calculated by averaging all of the individual ensemble member vector difference fields for each GCM (Figs. 9 and 14 later).

1) CCM3 VECTOR DIFFERENCE

Three important features are noted in the 1989 CCM3 ensemble mean composite difference: 1) a cyclonic flow anomaly northeast of the CP; 2) an anticyclonic anomaly west of the CP; and 3) a northeasterly flow anomaly

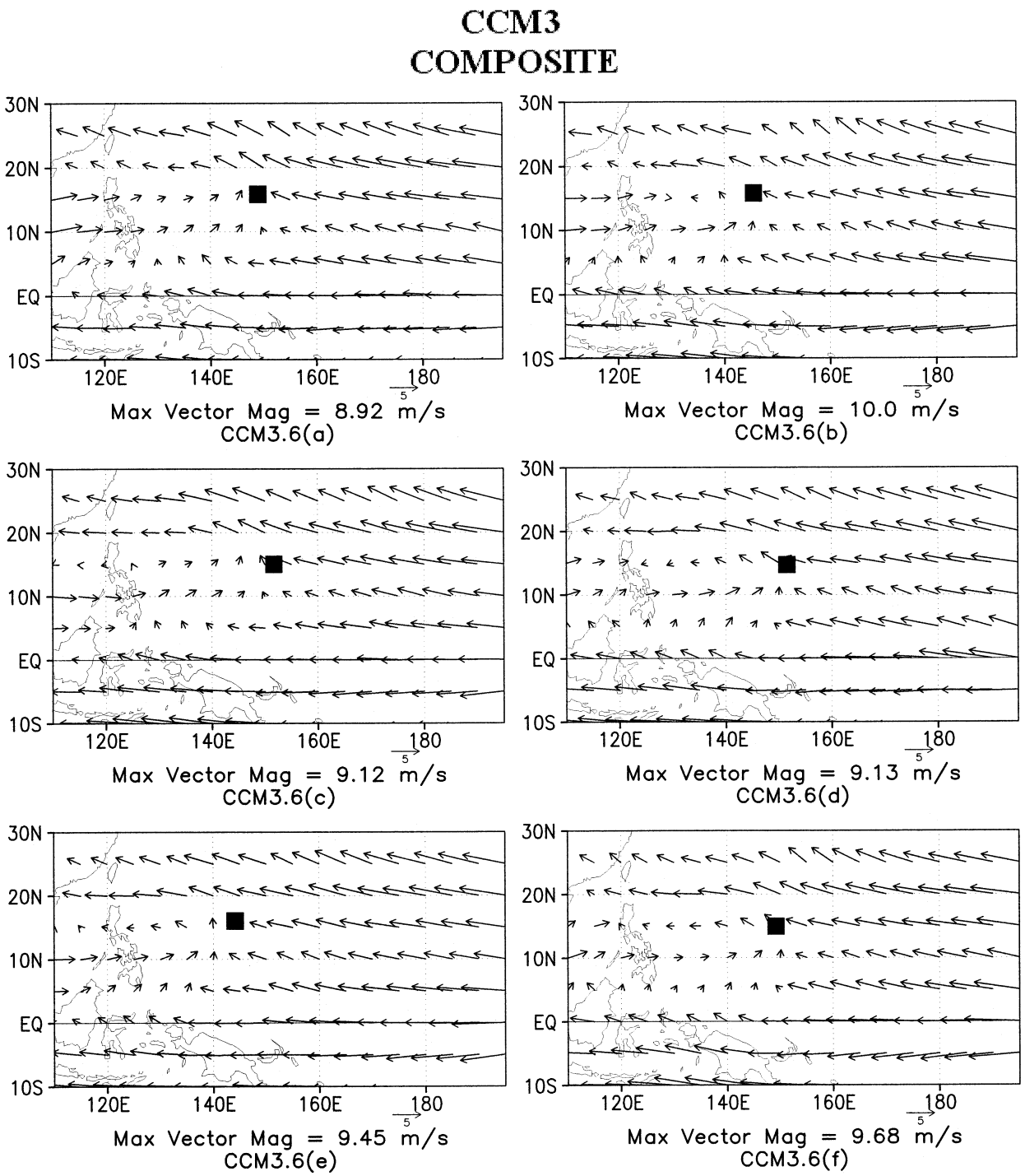

FIG. 7. CCM3 850-hPa wind composites for 1989 for each ensemble member. The solid square in each denotes the mean CP location for that ensemble member for the 1989 season.

southwest of the CP. The cyclonic anomaly northeast of the CP is related to the dislocation of the Pacific high. A westerly zonal wind anomaly of 1–1.5 m s^{-1} is observed south of the cyclonic anomaly in the TWT. This implies CCM3 is simulating a weaker easterly trade than observed. Typical easterly zonal winds are about 8 m s^{-1}, therefore, the westerly anomaly in the TWT is about 15% of the actual zonal wind speed. This result agrees with the result in Meehl and Arblaster (1998) where CCM3 (T42) shows an easterly anomaly near 10°N across the Pacific east of 140°E when it is compared with the NCEP reanalysis.

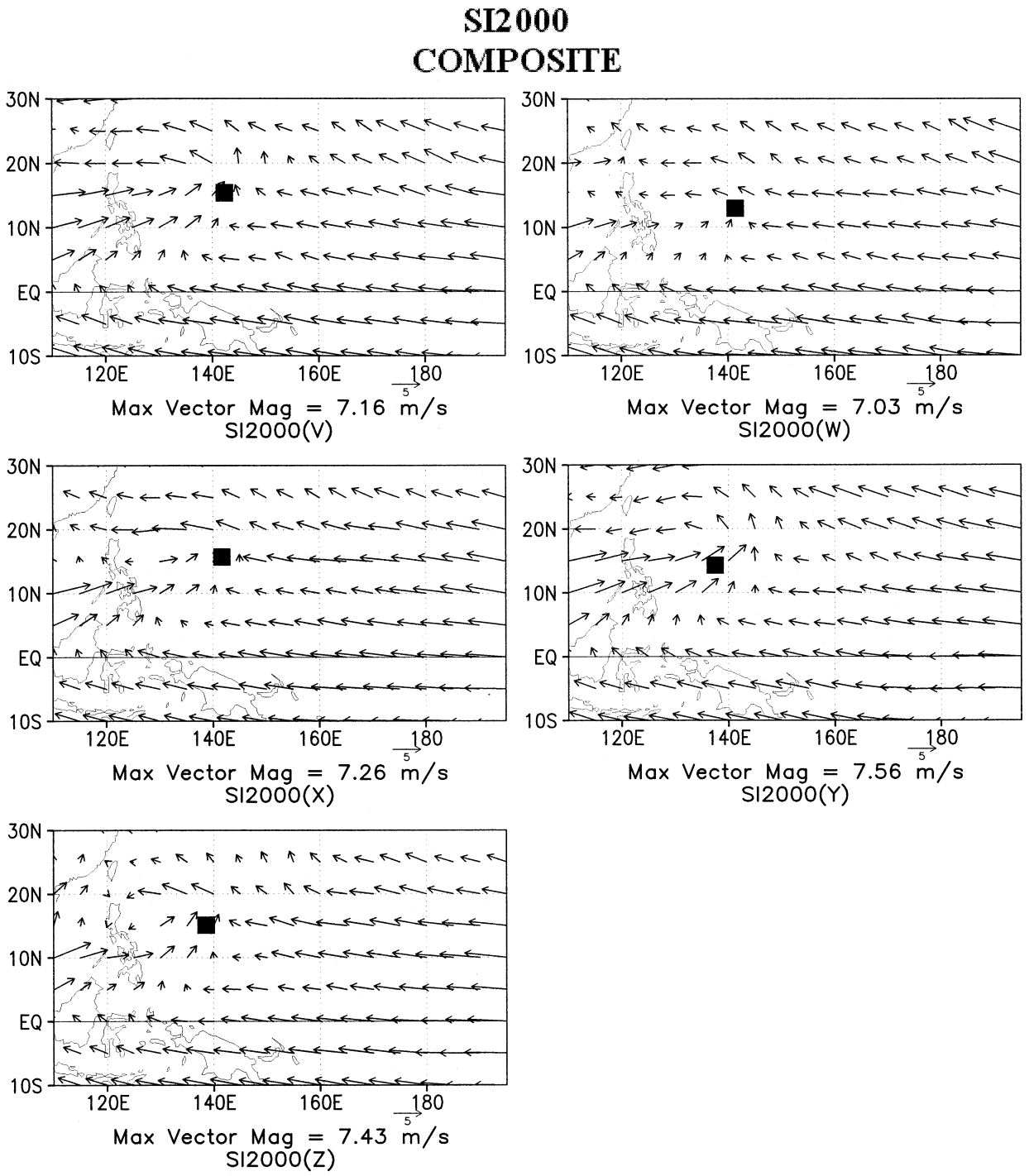

FIG. 8. SI2000 850-hPa wind composites for 1989 for each ensemble member. The solid square in each denotes the mean CP location for that ensemble member for the 1989 season.

To the west of the CP in the OMT, a cyclonic anomaly is seen extending from 110° to 140°E near 15°N with anomalous cross-equatorial northeasterly flow south of that cyclonic anomaly. Anomalous divergence of 1–3 $\times 10^{-6}$ s^{-1} is also seen on the northwestern side of this cyclonic anomaly and just to the west of the CP. This implies CCM3 is simulating a dynamically weaker OMT. A map of the rainfall anomalies (Fig. 10) shows that CCM3 significantly underestimates June–September total rainfall by up to 1200 mm from 110° to 160°E. This rainfall anomaly differs from the results in Meehl and Arblaster (1998), possibly due to the differing hor-

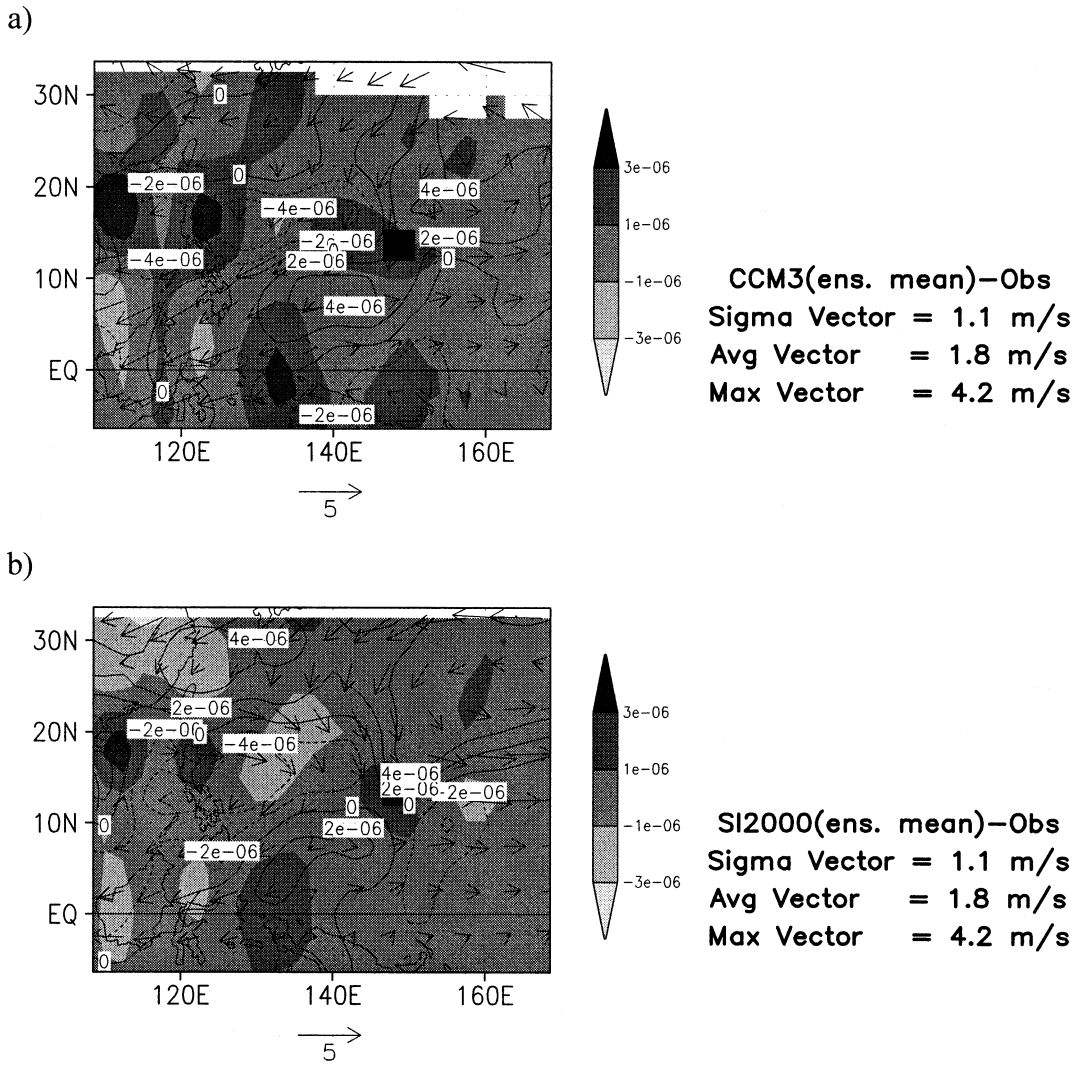

FIG. 9. Ensemble mean wind vector difference between (a) the ECMWF reanalysis and CCM3, and (b) the ECMWF reanalysis and SI2000 850-hPa wind composites for 1989. Contours represent vorticity with contour interval 2×10^{-6} s^{-1}. Shading represents divergence. The darkest shading denotes values greater than 3×10^{-6} s^{-1}, and the lightest shading denotes -3×10^{-6} s^{-1}. White background indicates regions in which a difference field could not be calculated from the available data.

izontal resolutions (T42 in Meehl and Arblaster 1998; cf. T31 here). The proportion of the anticyclonic anomaly that can be attributed to the lack of a realistic tropical cyclone climatology is not known. Anomalous divergence in the South China Sea is likely to provide dynamic forcing to reduce rainfall there, but it does not explain the extent of the rainfall anomaly. Anomalous cross-equatorial northeasterlies imply that CCM3 is simulating weaker monsoon southwesterlies, and weaker cross-equatorial southwesterlies in CCM3 imply a dynamically weaker east Asian monsoon. Anomalous northeasterlies extending from the cyclonic anomaly (associated with the dislocation of the Pacific high) from the northern Pacific into Indo-China are also found in Meehl and Arblaster (1998).

2) SI2000 VECTOR DIFFERENCE

SI2000 anomalies are qualitatively similar to CCM3: SI2000 shows a cyclonic anomaly northeast of the CP (related to dislocation of the Pacific high); an anticyclonic anomaly west of the CP, and a northeasterly flow anomaly southwest of the CP. The westerly zonal wind anomaly in the TWT is larger than the westerly flow anomaly in CCM3, up to about 3.5 m s^{-1}.

Similar to CCM3, SI2000 simulates an anticyclonic anomaly to the west of the CP and a northeasterly flow anomaly to the southwest of the CP. Unlike CCM3, SI2000 shows a stronger westerly anomaly on the north side of the anticyclonic anomaly, and the axis of the cyclonic anomaly northeast of the CP extends farther westward. Another difference between CCM3 and

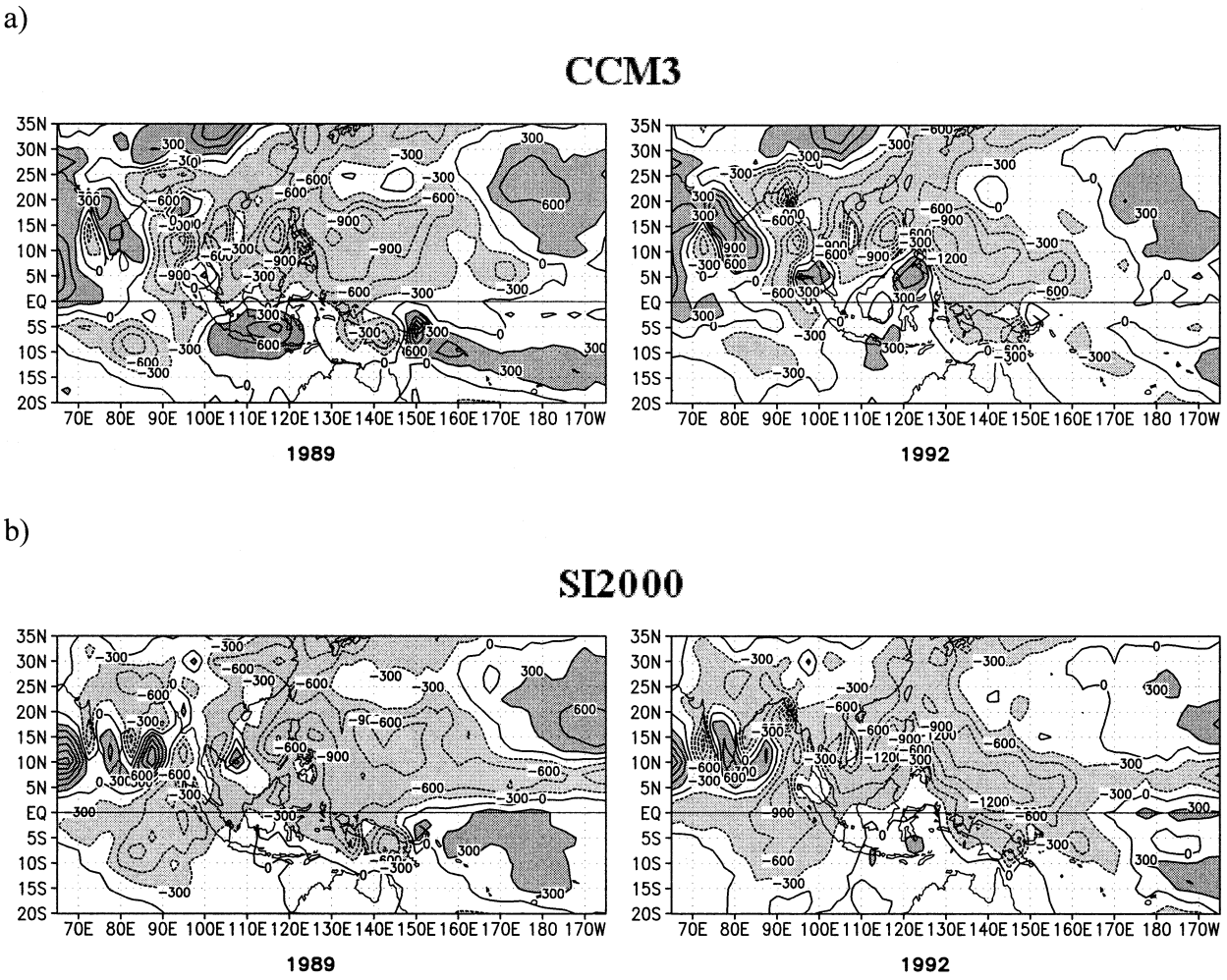

FIG. 10. Map of the 1989 and 1992 total seasonal rainfall anomalies for (a) CCM3, and (b) SI2000. Light shading indicates areas with more than 300-mm negative rainfall anomalies, and dark shading indicates areas with more than 300-mm positive rainfall anomalies. CCM3 significantly underestimates Jun–Sep total rainfall by up to 1200 mm from 110° to 160°E for 1992 (110°E to 180° for 1989). Anomalous divergence in the South China Sea likely suppresses the rainfall there, but does not explain the spatial extent of the anomaly. SI2000 also has negative Jun–Sep rainfall anomalies up to about 1200 mm in the OMT (which extends eastward past the date line), in spite of weaker divergence (or even convergence) anomalies in the OMT. Positive rainfall anomalies are noticed for both GCMs for both years in the subtropical central Pacific.

SI2000 can be seen in the divergence field; although SI2000 shows a divergent anomaly northwest of the anticyclonic anomaly, there is actually anomalous convergence in the northern part of the anticyclonic anomaly. This anomalous convergence is associated with the northerly flow to the northeast of the CP pushing into the eastern part of the anticyclonic anomaly. SI2000 also has negative total June–September rainfall anomalies up to about 1200 mm (Fig. 10), in spite of weaker divergence (or even convergence) anomalies in the 850-hPa OMT. Therefore, the large-scale divergence field cannot be the only reason for the rainfall anomalies observed in the OMT. South of the anticyclonic anomaly, SI2000 simulates a weaker cross-equatorial monsoon flow (anomalous northeasterly flow), but the magnitude of these anomalies is smaller in SI2000 than CCM3; this shows SI2000 has a better skill in simulating the monsoon southwesterlies, although both models underestimate the strength of the cross-equatorial monsoon flow.

b. Composite ITCZ structure for JJAS 1992

The ITCZ composites for 1992 are now evaluated the same way as in 1989. The 850-hPa vector wind composite for ECMWF reanalysis, CCM3 ensemble members, and SI2000 for 1992 are shown in Figs. 11, 12, and 13, respectively. The atmospheric response to the El Niño in progress pushes the CP farther to the east than in 1989. The ITCZ axis in both the ECMWF reanalyses and all but one CCM3 ensemble members (run e) show a northwest–southeast tilt in the OMT, while all SI2000 ensemble members are essentially zonal. In

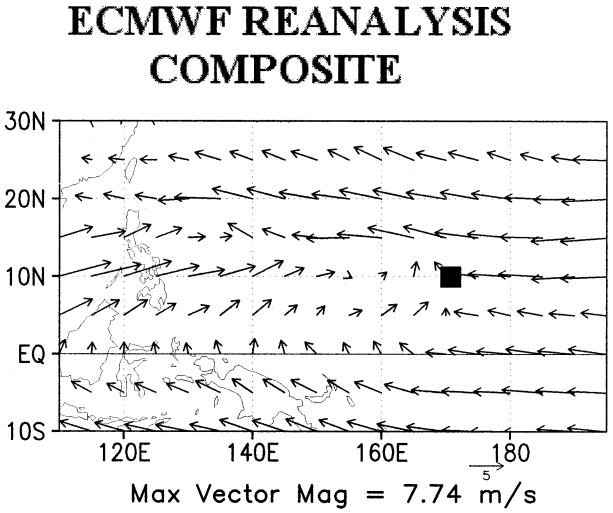

FIG. 11. ECMWF reanalysis 850-hPa wind composite for 1992. The solid square denotes the mean CP location for the season.

the TWT, CCM3 shows a stronger southerly meridional wind than in SI2000. Composites of some of the SI2000 ensemble members (runs W, X, and Z) show a double trough structure near the Asian continent in the northern part of the South China Sea. For the SI2000 ensemble members that do not show such a double trough structure, there is an area of very weak wind near 20°N in the South China Sea. The double trough structure in SI2000 is absent in both the ECMWF reanalysis and CCM3.

Ensemble mean vector differences between GCM ensemble members and the ECMWF reanalysis for 1992 are shown in Fig. 14. There are significant differences in the anomalous flow structures between 1989 and 1992, especially to the east and north of the CP.

1) CCM3 VECTOR DIFFERENCE

Unlike 1989, the cyclonic anomaly northeast of the CP is now moved to the east of the CP. A southeasterly flow anomaly is found northeast of the CP, and the westerly zonal wind anomaly in the TWT (also found in 1989) is located southeast of the CP, closer to the equator. The magnitude of the zonal wind anomaly southeast of the CP is up to about 1 m s^{-1}, so the trades in this El Niño year are better represented than in 1989.

The anticyclonic anomaly that existed to the west of the CP in 1989 appears as two separate anticyclonic anomalies in 1992, and associated with this anticyclonic anomaly is a divergent anomaly in the OMT and south of the OMT. The two anticyclonic anomalies are centered near (15°N, 135°E) and (10°N, 160°E). The anomaly to the northwest is associated with a divergence anomaly and a cross-equatorial northeasterly anomaly south of it. The northeasterly anomaly (which is also found in 1989) supports that CCM3 is simulating a weaker cross-equatorial southwesterly monsoon wind. Large negative rainfall anomalies are again seen in the OMT (Fig. 10), up to about 1200 mm (comparable to 1989) over the OMT and the South China Sea. This is consistent with the divergence anomaly seen on the OMT near (15°N, 135°E).

2) SI2000 VECTOR DIFFERENCE

For SI2000, westerly anomalies dominate to the north and east of the CP for 1992. The cyclonic anomaly that is seen in 1989 is evident in some of the ensemble members (runs V, X, Y and Z; not shown). Similar to 1989, the westerly anomaly east of the CP is up to about 3 m s^{-1}. Unlike CCM3, the westerly anomaly appears from 5°S to 25°N and is not limited to only the southeast of the CP.

To the west of the CP, SI2000 shows an anticyclonic anomaly. Similar to CCM3, two relative maxima of anticyclonic anomalies are identified, with one just to the west of the CP near (15°N, 160°E) and one centered near (15°N, 135°E). A divergent anomaly is observed near the former anticyclonic anomaly. Similar to 1989, anomalous northeasterly flow is seen south of that cyclonic anomaly. For 1992, the anomalous near-equatorial flow is more easterly in SI2000 than in CCM3. Unlike 1989, the magnitude of this anomalous flow is approximately the same for both CCM3 and SI2000 (3–3.5 m s^{-1}).

In general, both CCM3 and SI2000 simulate a dynamically weaker TWT (with consistently weaker easterly trade wind flow) and a dynamically weaker OMT (with an anticyclonic anomaly west of the CP). The anomalies in the OMT might be related to the lack of realistic tropical cyclones in the models. Both models simulate weaker monsoon southwesterlies south of the OMT and southwest of the CP.

8. Conclusions

The low-level (850 hPa) structure and the location of the ITCZ in the WPAC in CCM3 and SI2000 are investigated using ITCZ compositing and are compared with the structure of the ITCZ as seen in the ECMWF reanalysis. The ITCZ in the WPAC/CPAC can be divided into two main parts: the easterly trade wind trough (TWT) and the oceanic monsoon trough (OMT). The OMT and TWT are divided by the confluence point (CP) where monsoon westerlies turn sharply northward and easterly trades merge into the broad cyclonic flow in the OMT (Holland 1995). The OMT and CP are found to be a preferred region for tropical cyclone development (Briegel and Frank 1997; Ritchie and Holland 1999). Accurate simulations of the OMT and TWT have important implications to the energetics and the hydrological cycle in both GCMs, and are important to the understanding of the large-scale environment in which severe tropical weather is favorable.

The ITCZ is defined to be the 850-hPa relative vor-

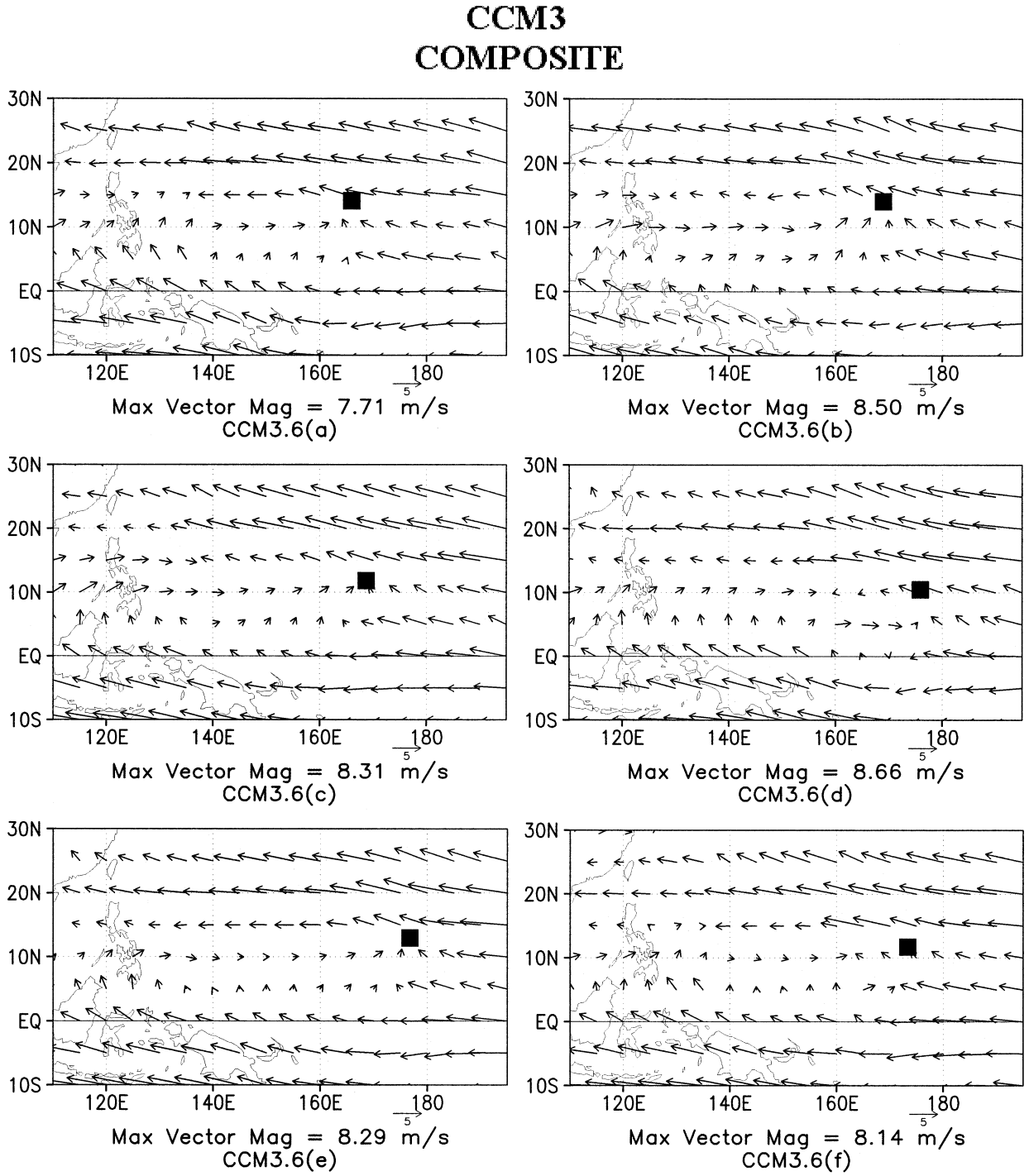

FIG. 12. CCM3 850-hPa wind composites for 1992 for each ensemble member. The solid square in each denotes the mean CP location for that ensemble member for the 1992 season.

ticity maximum, and the CP is defined to be a shift from an easterly trade regime to the cyclonic flow in the OMT. The ITCZ and the CP for both ECMWF reanalysis and GCMs are determined automatically using 850-hPa relative vorticity and zonal wind with a rule-based method with initial conditions determined visually from 850-hPa wind vector fields. The method uses two different ITCZ determination schemes (''well-defined'' trough scheme and ''poorly defined'' trough scheme; Chan 2001) to find the location of the ITCZ axis. The CP is determined by looking for a change of sign of the zonal wind south of the ITCZ axis. Only time periods during

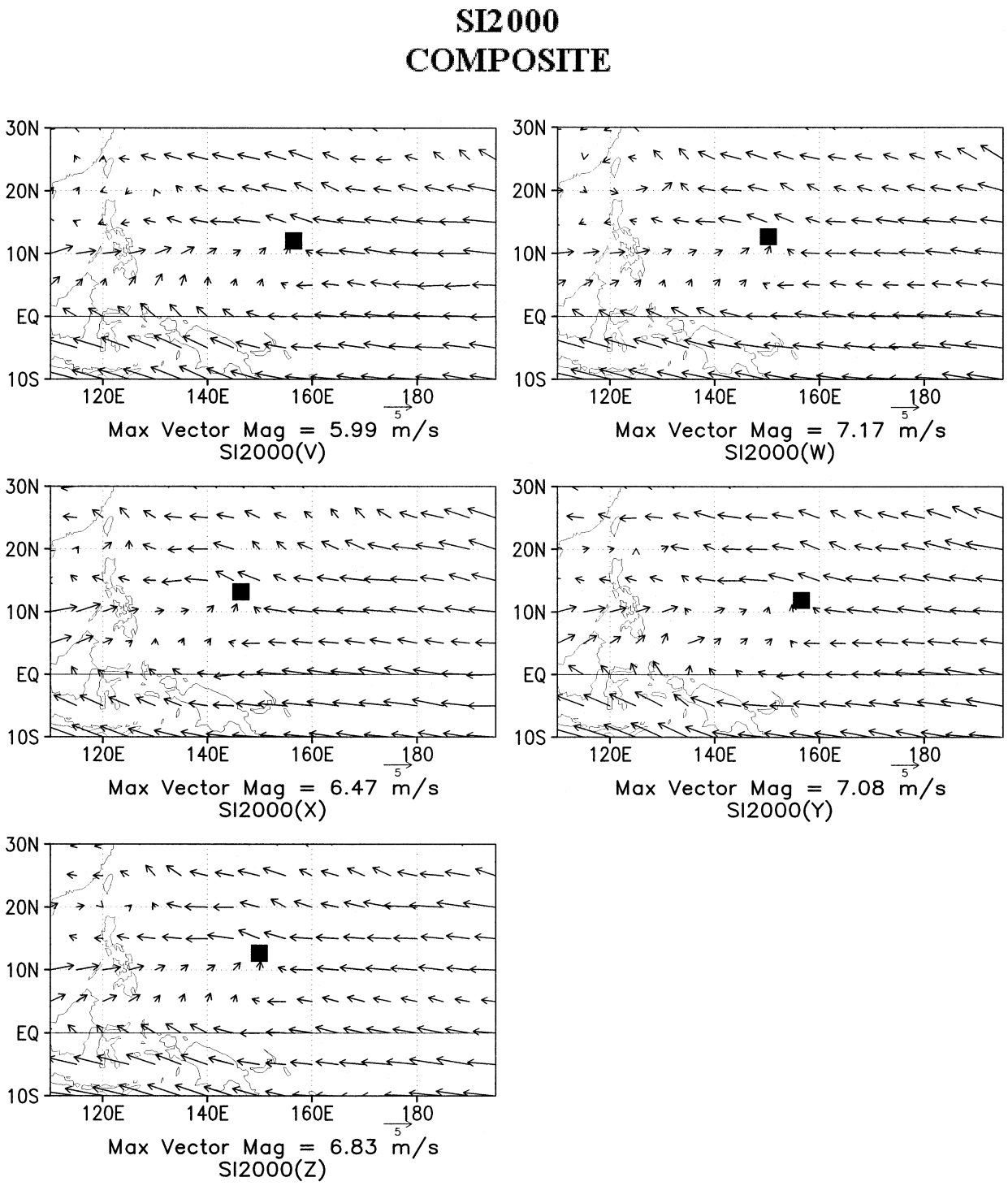

FIG. 13. SI2000 850-hPa wind composites for 1992 for each ensemble member. The solid square in each denotes the mean CP location for that ensemble member for the 1992 season.

the WPAC monsoon are considered in this study. The WPAC monsoon onset (retreat) is defined to be the development of westerly flow between 10° and 15°N east of 125°E.

Differences in the location of the ITCZ and the CP between the GCMs and ECMWF reanalysis are revealing. The CP in SI2000 shows a consistent west bias when compared with the ECMWF reanalysis. CCM3 shows no clear bias in longitude of the CP, but the CP for CCM3 is consistently north of the observed CP lo-

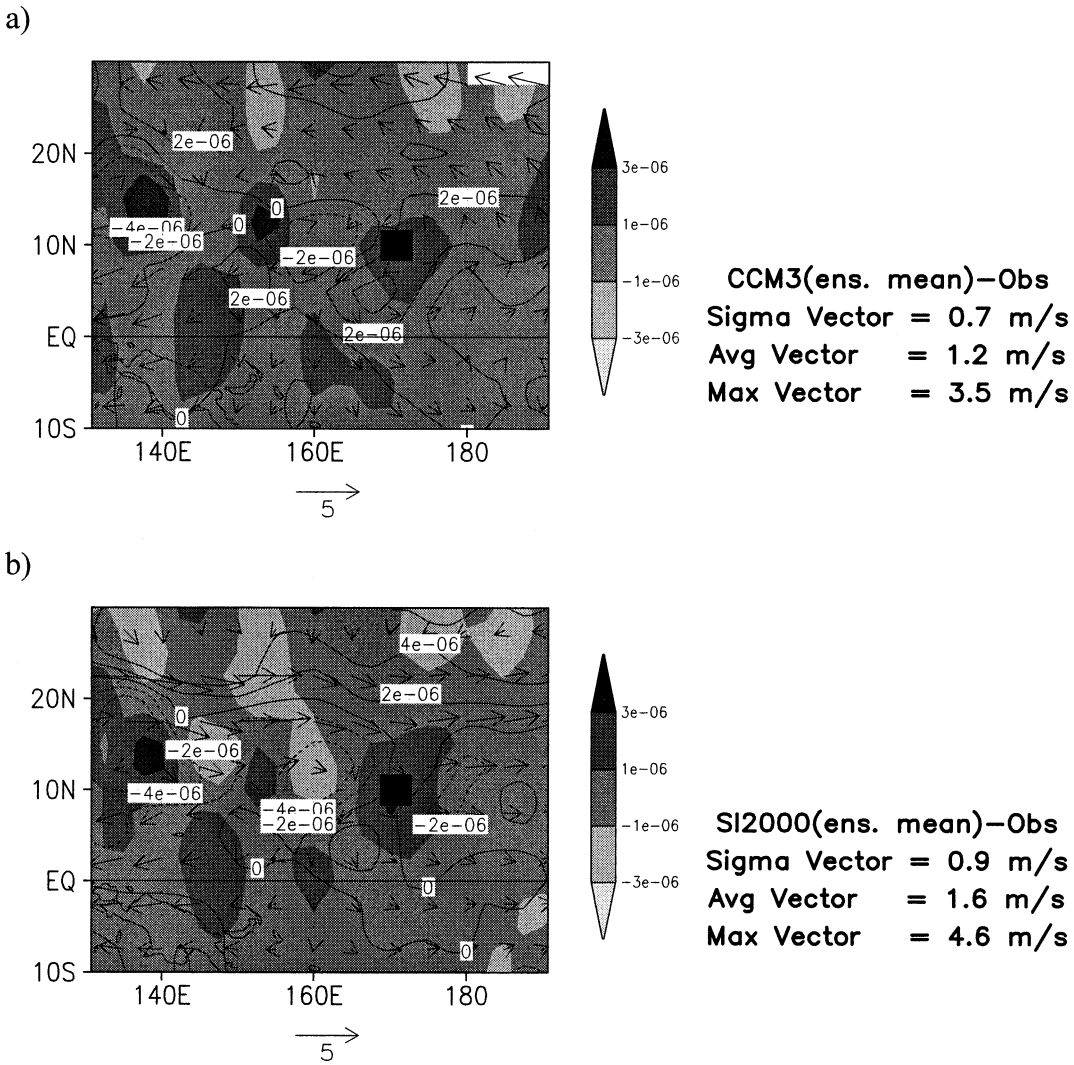

FIG. 14. Ensemble mean wind vector difference between (a) the ECMWF reanalysis and CCM3, and (b) the ECMWF reanalysis and SI2000 850-hPa wind composites for 1992. Contours represent vorticity with contour interval 2×10^{-6} s^{-1}. Shading represents divergence. The darkest shading denotes values greater than 3×10^{-6} s^{-1}, and the lightest shading denotes -3×10^{-6} s^{-1}. White background indicates regions in which a difference field could not be calculated from the available data.

cation. Both GCMs show skill in simulating the interannual variability of the mean CP longitude, but the spread of the CP longitudes for the years 1991–93 for CCM3 and 1992–93 for SI2000 are comparable with the movement of the ensemble mean CP location that is related to the ENSO events. Both GCMs show limited skill in simulating the northwest–southeast tilt of the ITCZ axis so both models' ITCZ is more zonal than observed.

The 850-hPa wind composites for both GCMs and the ECMWF reanalysis during 1989 and 1992 are calculated and compared. Both models simulate weaker easterly trades, and locate the Pacific high farther northeastward than observed. Both models simulate a weaker cross-equatorial monsoon southwesterly flow. SI2000 seems to show better skill in simulating the cross-equatorial monsoon flow than CCM3 for 1989, but this result cannot be reproduced for 1992. In the OMT, combined rainfall and wind vector differences suggest that both GCMs simulate a weaker than observed OMT. Anomalous anticyclonic flow is observed west of the CP, and large rainfall deficits are found there. CCM3 seems to show sensitivity to horizontal resolution in terms of the rainfall anomalies simulated in the OMT, since rainfall deficits that are found in the T31 runs analyzed here are not found in the T42 simulations documented by Meehl and Arblaster (1998).

In general, both GCMs show skill in simulating the structure of the ITCZ and its interannual variability. Biases do exist in some of the details of the ITCZ structure in the trades and the OMT, and large rainfall anomalies are noticed in the OMT. The underlying cause of

these biases is beyond the scope of this paper, but the identification of these biases can be used by climate forecasters when they are interpreting GCM climate forecasts. The compositing technique employed here can be used in other GCMs to ensure good quality control and predictability. As newer and improved GCMs become available in the future, similar GCM diagnostics can be employed to document the progress of GCM development. Low-level winds (Mapes and Houze 1995) are closely related to the deep convection in the tropical Pacific. As deep convection plays an important role in global atmospheric and oceanic energy budgets, more work is required to improve future GCMs for climate prediction and research in natural/human-induced climate change.

Acknowledgments. The authors thank Jan Dutton for the CCM3 data and James Hansen and colleagues at NASA Goddard for the SI2000 data. Robert Hart and George Tsakraklides provided valuable assistance with data management and graphics. Gregory Jenkins provided much helpful input through the life of this project.

APPENDIX

Analysis Methodology

a. ITCZ and confluence point (CP) determination

In this study, the ITCZ axis is defined to be a line of 850-hPa relative vorticity maximum between the equator and 30°N. The CP is defined to be the point where there is a shift of the zonal wind on the equatorward side of the trough axis. A shift of zonal wind is associated with the change from easterly trades to monsoon westerlies south of the CP. The methods of determining the location for both the OMT and CP are discussed here. Details of the techniques used in this study can also be found in Chan (2001). A general flow chart for the ITCZ axis and the CP location determination methodology is shown in Fig. A1.

1) INITIAL CONDITIONS

The first step of the analysis is the determination of the initial ITCZ axis and the CP locations for both the observations and the models. This is done by visually examining the 850-hPa wind vectors and vorticity fields of all ensemble members for each of the GCMs and the ECMWF reanalysis. These locations are used for the initial time period (0000 UTC 1 June) for each year in each ensemble member for each GCM and the ECMWF reanalysis. This initial ITCZ information is also used as initial conditions for the rule-based ITCZ determination routine (to be described below).

After the initial ITCZ and CP location is determined, this initial ITCZ information and the 12-hourly ECMWF/GCM data are sent to a rule-based ITCZ determination routine. Unlike the initial ITCZ and monsoon onset time that are determined by visual examination, the rule-based ITCZ determination routine is automatic to ensure good efficiency and speed.

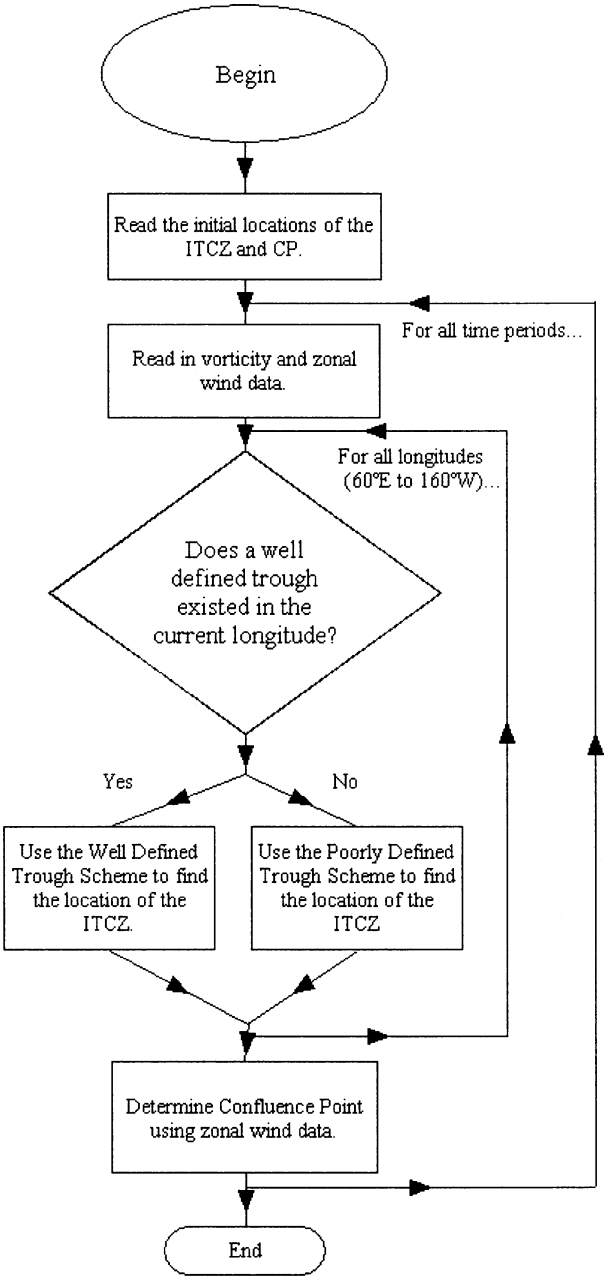

FIG. A1. Flow chart of the general methodology of determination of the ITCZ axis and CP location. Note that first guesses of the ITCZ axis and CP locations are required input to this routine.

2) DETERMINATION OF THE ITCZ AXIS: WELL-DEFINED TROUGH VERSUS POORLY DEFINED TROUGH

Beginning from the easternmost longitude (160°W) and going westward, the procedure first tries to deter-

mine the existence of a ''well-defined'' trough. A well-defined trough is defined as a cyclonic low pressure trough that is at least 7.5° latitude wide; this criterion is called the ''width criterion'' for a well-defined trough. Apart from the width criterion, there is a ''location criterion'' to ensure there are no large breaks in the ITCZ axis both spatially and temporally. In order to satisfy the location criterion, a well-defined trough has no more than 5.0° latitude displacement from the ITCZ axis east of the current longitude; neither a well-defined trough has more than 7.5° latitude displacement from the ITCZ axis on the same longitude from the previous time period. In order to employ the location criterion, an initial ITCZ axis for the first time period (0000 UTC 1 June) must be defined. For 160°W (easternmost longitude within the domain of interest), the ITCZ axis just east is assumed to be 5°N; this assumption is based on observational studies from Waliser and Gautier (1993).

If a well-defined trough(s) exists, the ''well-defined trough'' scheme will be used to determine the location of the ITCZ axis. In the first pass through, the 12-hourly data, the scheme determines if there are two or more well-defined troughs. If there is only one well-defined trough, that well-defined trough is automatically chosen to be the ITCZ axis. If there are two or more well-defined troughs, the meridional displacement of each well-defined trough from the ITCZ axis east of the current longitude is determined. The trough with the less meridional displacement is chosen to be the ITCZ axis. If there are two well-defined troughs with the same meridional displacement, the trough with the least meridional displacement from the equator or 30°N is chosen to be the ITCZ axis.

At longitudes with no well-defined troughs, the ''poorly defined'' trough scheme is used to determine the location of the ITCZ axis. The poorly defined trough scheme searches for three distinct positive relative vorticity maxima from the latitudes that are within 5.0° latitude of the ITCZ axis east of the current longitude. The location of the vorticity maximum with the least meridional displacement from the ITCZ axis east of the current longitude is determined. This location is then designated to be the ITCZ axis. In the case of no qualifying relative vorticity maxima, the latitude of the ITCZ axis is assumed to be the midpoint between the ITCZ axis east of the current longitude and the ITCZ axis from the previous time period on the same longitude.

This step is repeated until the ITCZ axis of the whole spatial domain is determined. After completion, the location of the CP can now be determined.

3) The location of the confluence point

Beginning from 160°W and going westward, the CP is determined by finding a change of sign of the zonal wind south of the ITCZ axis. In order to filter out the changes of sign of zonal wind due to spatially local phenomena, a six-gridpoint spatially averaged zonal wind to the south and southwest of the current longitude is computed. The longitude of CP is constrained to be no farther west than 110°E; if the CP cannot be found east of 110°E, the CP is assumed to be 110°E.

4) The ITCZ axis for the whole JJAS

The procedures described in sections 2 and 3 are repeated until the 12-hourly ITCZ of JJAS of 1989–93 is completely determined. The ITCZ axis locations are then stored, and are ready for use for composite analysis.

b. Composite technique

The composite technique is originally developed for a tropical cyclone study (Briegel and Frank 1997), and is modified for the use of this study. A flow chart on the compositing technique is shown in Fig. A2.

1) Time-mean CP location

The first step is to determine the mean location of the CP. With a given time range (between the monsoon onset and retreat), the mean longitude and latitude of the CP is calculated with a simple arithmetic mean. This mean CP location serves as a ''center point'' (to be explained) for the composite mean ITCZ axis and remapping of wind maps.

2) Composite mean ITCZ axis

The 12-hourly CP (and the ITCZ axis that is associated with it) is then centered onto the mean CP location. After centering, a composite mean ITCZ axis is then computed.

Consider a CP location of any 12-hourly period, there is a certain meridional and zonal displacement from the mean CP location that is computed in determining the time-mean CP location. This CP location (and its associated ITCZ axis) is moved to the mean CP location. The moving of the 12-hourly CP centers the 12-hourly ITCZ axis onto the mean CP locations. This ITCZ axis centering is performed for all times of interest. This centering procedure separates the easterly trade wind region and the monsoon trough at the mean CP location; east of the mean CP location are the trade wind regions of the centered 12-hourly ITCZ axis, west of all the mean CP location is the monsoon trough of the centered 12-hourly ITCZ axis.

For each longitude, the time-mean latitude of the centered ITCZ axis is computed. This step constructs a new ITCZ axis with a CP equals to the time-mean CP location. This new ITCZ axis is defined to be the composite mean ITCZ axis.

3) Remapping and compositing

The composite mean ITCZ axis is likely to differ from the 12-hourly CP-centered ITCZ axis in terms of the latitude of the ITCZ axis at each longitude. This lati-

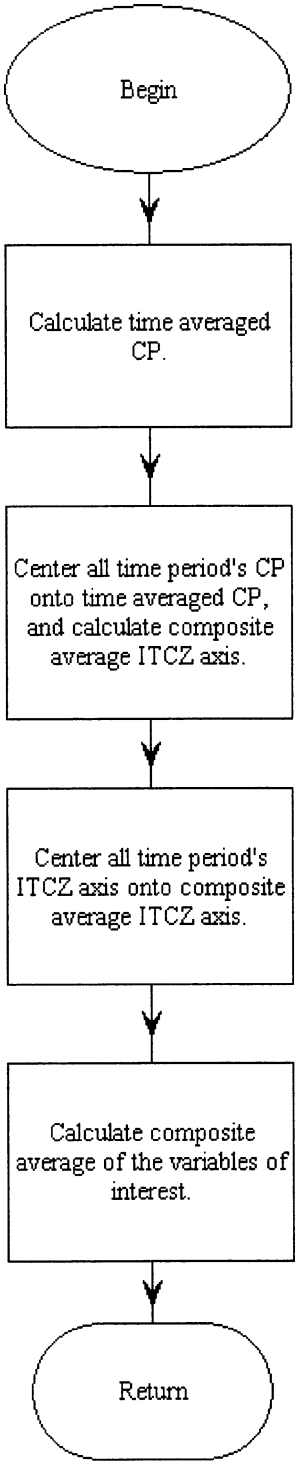

FIG. A2. Flow chart of the method used to construct the ITCZ composites.

tudinal displacement between the 12-hourly CP-centered ITCZ and the composite mean ITCZ is computed. This displacement is used for remapping of the 12-hourly variable maps (e.g., a map of 850-hPa zonal wind).

How the 12-hourly variable map is remapped is similar to how the 12-hourly ITCZ axis is centered onto the time-mean CP location. Instead of the ITCZ axis being centered upon the time-mean CP location, the variable map is the one being centered. The whole 12-hourly variable map moves with the 12-hourly CP location, so that the 12-hourly CP overlaps with the time-mean CP location. The centering separates features on the variable map that are associated with the trade winds and the monsoon trough with the time-mean CP location.

Each longitude on the CP-centered variable map is moved meridionally by the latitudinal displacement between the composite mean ITCZ axis and the 12-hourly CP-centered ITCZ. This centers the variable map onto the composite mean ITCZ axis, and separates features on the variable map that are north or south of the ITCZ axis. The remapping of the 12-hourly variable map is now complete.

This remapping is done for all times of interest. The remapping overlays different 12-hourly variable maps that are now all centered onto the composite mean ITCZ axis. A mean of the all centered variable map is computed, and this new variable map is the composite mean variable map.

REFERENCES

Abramopoulos, F., 1991: A new fourth-order enstrophy and energy conserving scheme. *Mon. Wea. Rev.*, **119,** 128–133.

Boville, B., 1991: Sensitivity of simulated climate to model resolution. *J. Climate*, **4,** 469–485.

Briegel, L., and W. M. Frank, 1997: Large-scale influences on tropical cyclogenesis in the western North Pacific. *Mon. Wea. Rev.*, **125,** 1397–1413.

Chan, S. C., 2001: Composite structure and variability of the Eastern Hemisphere's ITCZ during boreal summer in ECMWF re-analysis, CCM 3.6 and SI2000 general circulation models. M.S. thesis, Dept. of Meteorology, The Pennsylvania State University, 107 pp. [Available from Dept. of Meteorology, The Pennsylvania State University, 503 Walker Building, University Park, PA 16802.]

Chang, C. P., and G. T. J. Chen, 1995: Tropical circulations associated with southwest monsoon onset and westerly surges over South China Sea. *Mon. Wea. Rev.*, **123,** 3254–3267.

Chang, H. R., and P. J. Webster, 1990: Energy accumulation and emanation at low latitudes. Part II: Nonlinear response to strong episodic equatorial forcing. *J. Atmos. Sci.*, **47,** 2624–2644.

Columbia University, cited 2001: IRI/LDEO online climate data library. [Available online at http://ingrid.ldgo.columbia.edu/.]

Deardorff, J. W., 1972: Parameterization of the planetary boundary layer for use in general circulation models. *Mon. Wea. Rev.*, **100,** 93–106.

Del Genio, A., and M. S. Yao, 1993: Efficient cumulus parameterization for long-term climate studies: The GISS scheme. *The Representation of Cumulus Convection in Numerical Models, Meteor. Monogr.*, No. 46, 181–184.

Dutton, J., and E. Barron, 2000: Intra-annual and interannual ensemble forcing of a regional climate model. *J. Geophys. Res.*, **105,** 523–529.

Engelen, R. J., I. L. Wittmeyer, and G. L. Stephens, 1998: Assessment of reanalysis hydrology and energy budgets: Water vapor and radiative fluxes. *Proc. First Int. WCRP Conf. on Reanalysis,*

Silver Spring, MD, World Climate Research Programme, WCRP-104 (WMO/TD-876), 175–178.
Fennessy, M. J., and Coauthors, 1994: The simulated Indian monsoon: A GCM sensitivity study. *J. Climate,* **7,** 33–43.
Gadgil, S., and A. Guruprasad, 1990: An objective method for the identification of the intertropical convergence zone. *J. Climate,* **3,** 558–567.
——, and S. Sajani, 1998: Monsoon precipitation in the AMIP runs. *Climate Dyn.,* **14,** 59–689.
Gates, W., and Coauthors, 1999: An overview of the results of the Atmospheric Model Intercomparison Project (AMIP I). *Bull. Amer. Meteor. Soc.,* **80,** 29–56.
Gibson, J. K., P. Kållberg, S. Uppala, A. Hernandez, A. Nomura, and E. Serrano, 1997: ERA description. Reanalysis (ERA) Project Report Series, No. 1, European Centre for Medium-Range Weather Forecasts, 74 pp.
Gray, W. M., 1968: Global view of the origin of tropical disturbances and storms. *Mon. Wea. Rev.,* **96,** 669–700.
Hansen, J., and Coauthors, 1997: Forcings and chaos in interannual to decadal climate change. *J. Geophys. Res.,* **102,** 25 679–25 720.
Hartke, G., and D. Rind, 1997: Improved surface and boundary layer models for the Goddard Institute for Space Studies general circulation model. *J. Geophys. Res.,* **102,** 16 407–16 422.
Holland, G., 1995: Scale interaction in the western Pacific monsoon. *Meteor. Atmos. Phys.,* **56,** 57–79.
Holtslag, A. A. M., and B. A. Boville, 1993: Local versus nonlocal boundary-layer diffusion in a global climate model. *J. Climate,* **6,** 1825–1842.
Kiehl, J. T., and D. L. Williamson, 1991: Dependence of cloud amount on horizontal resolution in the National Center for Atmospheric Research Community Climate Model. *J. Geophys. Res.,* **96,** 10 955–10 980.
——, J. J. Hack, G. B. Bonan, B. A. Boville, B. Briegleb, D. L. Williamson, and P. J. Rasch, 1996: Description of the NCAR Community Climate Model (CCM3). National Center for Atmospheric Research Tech. Note 420+STR, 160 pp.
——, ——, ——, ——, D. L. Williamson, and P. J. Rasch, 1998: The National Center for Atmospheric Research Community Climate Model: CCM3. *J. Climate,* **11,** 1131–1149.
Lau, K. M., and M. T. Li, 1984: The monsoon of east Asia and its global associations—A survey. *Bull. Amer. Meteor. Soc.,* **65,** 114–125.
——, and S. Yang, 1996: Seasonal variation, abrupt transition, and intraseasonal variability associated with the Asian summer monsoon in the GLA GCM. *J. Climate,* **9,** 965–985.
——, J. H. Kim, and Y. Sud, 1996: Intercomparison of hydrologic processes in AMIP GCMs. *Bull. Amer. Meteor. Soc.,* **77,** 2209–2228.
Laval, K., R. Raghava, J. Polcher, R. Sadourny, and M. Forichon, 1996: Simulations of the 1987 and 1988 Indian monsoon using the LMD GCM. *J. Climate,* **9,** 3357–3371.
Lean, J., 2000: Evolution of the sun's spectral irradiance since the Maunder Minimum. *Geophys. Res. Lett.,* **27,** 2425–2428.
Madden, R., and P. Julian, 1972: Description of global scale circulation cells in the tropics with a 40–50 day period. *J. Atmos. Sci.,* **29,** 1109–1123.
Mapes, B. E., and R. A. Houze, 1995: Diabatic divergence profile in western Pacific mesoscale convection systems. *J. Atmos. Sci.,* **52,** 1807–1828.
Matsuno, T., 1966: Quasi-geostrophic motions in the equatorial area. *J. Meteor. Soc. Japan,* **44,** 25–42.
Meehl, G., and J. M. Arblaster, 1998: The Asian–Australian monsoon and El Niño–Southern Oscillation in the NCAR Climate System Model. *J. Climate,* **11,** 1356–1385.
Newman, M., P. D. Sardeshmukh, and J. W. Bergman, 2000: An assessment of the NCEP, NASA, and ECMWF reanalyses over the tropical west Pacific warm pool. *Bull. Amer. Meteor. Soc.,* **81,** 41–48.
Philander, S. G. H., D. Gu, G. Lambert, T. Li, D. Halpern, N.-C. Lau, and R. C. Pacanowski, 1996: Why the ITCZ is mostly north of the equator. *J. Climate,* **9,** 2958–2972.
Plante, R. J., and C. P. Guard, 1989: 1989 annual tropical cyclone report. Joint Typhoon Warning Center, 254 pp.
Ramage, C. S., 1971: *Monsoon Meteorology.* Academic Press, 296 pp.
Rayner, N., 2000: HadlSST1 sea ice and sea surface temperature data files. Hadley Center, Bracknell, Berkshire, United Kingdom. [Available online at http://www.met-office.gov.uk/research/hadleycentre/obsdata.]
Reynolds, R. W., and T. M. Smith, 1994: Improved global sea surface temperature analyses using optimum interpolation. *J. Climate,* **7,** 929–948.
Ritchie, E., and G. J. Holland, 1999: Large-scale patterns associated with tropical cyclogenesis in the western Pacific. *Mon. Wea. Rev.,* **127,** 2027–2043.
Sadler, J. C., 1975: The monsoon circulation and cloudiness over the GATE area. *Mon. Wea. Rev.,* **103,** 369–387.
Slingo, J. M., and Coauthors, 1994: Mean climate and transience in the tropics of the UGAMP GCM: Sensitivity to convective parameterization. *Quart. J. Roy. Meteor. Soc.,* **120,** 881–922.
Smith, T. M., R. W. Reynolds, R. E. Livezey, and D. C. Stokes, 1996: Reconstruction of historical sea surface temperatures using empirical orthogonal functions. *J. Climate,* **9,** 1403–1420.
Sperber, K. R., S. Hameed, G. L. Potter, and J. S. Boyle, 1994: Simulation of the northern summer monsoon in the ECMWF model: Sensitivity to horizontal resolution. *Mon. Wea. Rev.,* **122,** 2461–2481.
Tao, S., and L. Chen, 1987: A review of recent research of the East Asian summer monsoon in China. *Monsoon Meteorology,* C. G. Chang and T. N. Krishnamurti, Eds., Oxford University Press, 60–92.
Trenberth, K. E., and C. J. Guillemot, 1998: Evaluation of the atmospheric moisture and hydrological cycle in the NCEP/NCAR reanalyses. *Climate Dyn.,* **14,** 213–231.
——, D. P. Stepaniak, J. W. Hurrell, and M. Fiorino, 2001: Quality of reanalyses in the Tropics. *J. Climate,* **14,** 1499–1510.
Vogelezang, D. H. P., and A. A. M. Holtslag, 1996: Evaluation and model impacts of alternative boundary-layer height formulation. *Bound.-Layer Meteor.,* **81,** 245–269.
Waliser, D., and C. Gautier, 1993: A satellite-derived climatology of the ITCZ. *J. Climate,* **6,** 2162–2174.
Webster, P. J., 1981: A model of the planetary scale monsoon. *Monsoon Dynamics,* J. Lighthill and R. Pearce, Eds., Cambridge University Press, 165–192.
Wheeler, M., G. N. Kiladis, and P. J. Webster, 2000: Large-scale dynamical fields associated with convectively coupled equatorial waves. *J. Atmos. Sci.,* **57,** 613–640.
Wu, R., and B. Wang, 2001: Multi-stage onset of the summer monsoon over the western North Pacific. *Climate Dyn.,* **17,** 277–289.
Zhang, G. J., and N. A. McFarlane, 1995: Sensitivity of climate simulations to the parameterization of cumulus convection in the Canadian Climate Centre general circulation model. *Atmos.–Ocean,* **33,** 407–446.